

# Multicopter with Series Connected Propeller Drives

Florian Bauer, *Member, IEEE*, Christoph M. Hackl, *Senior Member, IEEE*, Keyue Smedley, *Fellow, IEEE*, and Ralph M. Kennel, *Senior Member, IEEE*

**Abstract**—This study considered a tethered multicopter, powered from ground by electrical cables integrated in the tether. For a low tether mass and diameter, but high-efficient and simple propeller drives, a higher tether voltage than the rated voltage of the propeller drives was considered. To avoid additional power converters to step-down the tether voltage, the propeller drives were proposed to be connected partly in series. A control method was developed to stabilize the voltages and simultaneously achieve the requested propeller forces and moments. The feasibility of the proposed concept and the effectiveness of the developed control method were demonstrated by experiments. The proof-of-principle demonstrator was a tethered octocopter with 48 V tether voltage, wherein two or four voltage levels were created by a series connection. The demonstrator flew stably for several minutes until a test flight was completed successfully. During flight, the voltage control errors were always less than 0.75 V. A possible application of such a system with a scaled-up voltage is crosswind kite power where the kite is equipped with small onboard turbines and the electricity is transmitted to the ground via electrical cables. During launching and landing, the turbines are used as propellers, i.e. the kite is a tethered multicopter and hovers from ground into a launching position, or vice versa.

**Index Terms**—Multicopter, drive, voltage source converter, series connection, kite.

## I. MOTIVATION

**M**ULTICOPTERS are propeller-equipped vertical take-off and landing (VTOL) aircraft. One application of commercially available multicopters with a size in the magnitude of 1 m is aerial imaging. Usually each propeller is mounted to a three-phase brushless motor (brushless DC motor, BLDC, or permanent magnet synchronous machine, PMSM) which is driven by an “electronic speed controller” (ESC), i.e. a three-phase voltage source converter (VSC). The DC terminals of the VSCs are all connected in parallel and supplied by a battery with a low voltage in the magnitude of  $\leq 60$  V.

© 2017 IEEE. Personal use of this material is permitted. Permission from IEEE must be obtained for all other uses, in any current or future media, including reprinting/republishing this material for advertising or promotional purposes, creating new collective works, for resale or redistribution to servers or lists, or reuse of any copyrighted component of this work in other works.

This is the preprint of the accepted paper F. Bauer; C. M. Hackl; K. M. Smedley; R. M. Kennel, “Multicopter With Series Connected Propeller Drives,” in IEEE Transactions on Control Systems Technology, DOI: 10.1109/TCST.2017.2679071, URL: <http://ieeexplore.ieee.org/document/7888441/>

Florian Bauer is Ph.D. candidate at the Institute for Electrical Drive Systems and Power Electronics, Technical University of Munich, Arcisstrasse 21, 80333 Munich, Germany, [florian.bauer@tum.de](mailto:florian.bauer@tum.de), corresponding author.

Christoph M. Hackl is Head of the Research Group “Control of Renewable Energy Systems” at the Munich School of Engineering/Technical University of Munich, c/o Wind Energy Institute, Boltzmannstrasse 15, 85748 Garching, Germany.

Keyue Smedley is Professor at The Henry Samueli School of Engineering, Power Electronics Laboratory, University of California, Irvine, CA, 92697.

Ralph M. Kennel is Professor at the Institute for Electrical Drive Systems and Power Electronics, Technical University of Munich, Arcisstrasse 21, 80333 Munich, Germany.

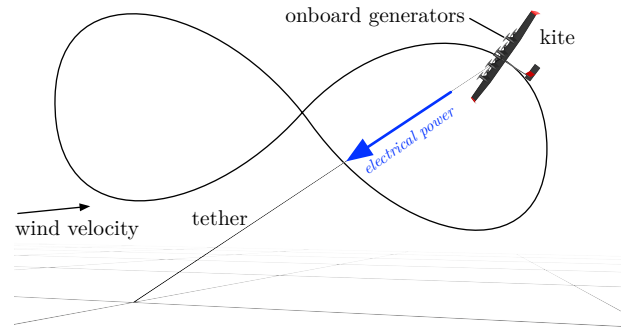


Fig. 1. Illustration of “drag power”.

Another application of multicopters is recently being studied: Fig. 1 shows the crosswind kite power concept “drag power” (also called “onboard-”, “continuous power generation”, “fly-gen”, or “airborne wind turbine”, see e.g. [1], [2]). The kite (i.e. tethered wing/glider) is flown in fast crosswind trajectories like figure eights or circles. The kite has onboard wind turbines and generators to generate electrical power. Due to the high speed of the kite, the airspeed at the kite is about a magnitude higher than the actual wind speed, so that the onboard turbines can be small. The electrical power is transmitted to the ground via cables integrated in the tether. For minimal tether mass and aerodynamic losses, a medium voltage in the magnitude of 10 kV is chosen [3]. Before the kite flies in crosswind trajectories, the generators and wind turbines are used as motors and propellers for a vertical take-off and subsequent transition into crosswind flight. The reverse procedure is used for the landing when the wind calms down or for maintenance. During these launching and landing phases, the kite is a tethered multicopter. Compared to conventional wind turbines, crosswind kite power promises to harvest wind energy at higher altitudes with stronger and steadier winds, but requires only a fraction of the construction material. Hence, it promises to have a higher capacity factor, lower capital investments, and in the end a lower leveled cost of electricity (LCOE). A drag power kite with a rated electric power of 20 kW was developed by the company Makani Power/Google and demonstrated autonomously all flight maneuvers and power generation [2, Chap. 28]. Currently, a 600 kW system is being developed [4].

Due to the high tether voltage, it is not desirable to use a simple parallel connection of the VSCs of the electrical drives<sup>1</sup> as for small multicopters: (i) Relatively thick isolations would

<sup>1</sup>Throughout this paper, the term “drive” denotes the combination of electrical machine (motor/generator), its power electronics and its current-, torque- and angular speed controllers.

be required for the coil wires of the electrical machines and thus would reduce efficiency and/or the torque- and power-to-weight-ratio. (ii) A VSC with such a high voltage rating would require a multilevel topology and thus would be costly and complex. Similar conclusions were made by Kolar et al. in [3]: They proposed to use several 8 kV-to-700 V bidirectional DC-DC converters based on a dual active bridge (DAB). However, drawbacks are the additional mass, development and manufacturing costs, electromagnetic interference (EMI) or additional possible points of failure.

This study considered a different approach: A mix of series and parallel connections of the VSCs of the propeller drives was proposed with little to no special design considerations on the VSCs. It was still considered, that only two DC potentials lead to the kite in the tether. Consequently, the series connection created additional voltage levels on the kite and their voltages were coupled to the propellers' power consumption (or generation) and thus propeller forces and torques.

Connecting electrical drives in series has been studied recently for tower-based offshore wind turbines to avoid an offshore converter station: One concept considers series connected current source converters (CSCs) (see e.g. [5]–[7]), which are as independent as parallel connected VSCs. CSCs may also be an alternative for the turbines/propellers of a drag power kite, however CSCs are more complex and costly, and thus usually not preferred for electrical drives. Another concept also considers series connected VSCs (see e.g. [8]–[10]). A challenge for both concepts is the insulation for the very high DC-voltage in the magnitude of a few 100 kV, because the generator irons and thus the nacelles should be grounded e.g. for safety reasons. This is proposed to be solved by a generator-side transformer for CSCs and isolated DC-DC-converters for VSCs. This study considers isolation not as an issue for a drag power kite, as the voltage is a magnitude lower and there is no obvious requirement for grounding the generator irons. Contrary to a kite, the torque and thrust generated by any tower-based wind turbine is compensated by the tower and is thus irrelevant for the control of power or voltages. The control of a multicopter is already well studied (cf. e.g. [11]–[14] and references therein). However, no study was found which considers a series connection of propellers/wind turbines of a flying vehicle. On the contrary, Kolar et al. ruled out a series connection in [3].

This study considered a tethered multicopter, powered from ground by cables integrated in the possibly long tether for infinite flight time. As a possible application is a drag power kite, this study can be seen as a first evaluation of the idea of series connected VSC-wind turbine/propeller drives by considering only the launching and landing maneuvers where the kite is a multicopter. The contributions of this study can be summarized as follows:

- (i) Proposal of series connected propeller drives for multicopters,
- (ii) formulation of a generalized and simplified electro-mechanical model,
- (iii) development of a stabilizing voltage and attitude controller, and
- (iv) verification through experiments.

This study is organized as follows: Sec. II discusses topologies of series connected VSCs and propeller drives as well as possible control actuations. Sec. III derives the model equations and formulates the control problem. Sec. IV proposes a solution and Sec. V reports measurement results of a demonstrator. Finally, Sec. VI gives conclusions and an outlook.

## II. TOPOLOGIES WITH SERIES CONNECTED VSC-PROPELLER DRIVES

### A. Approximation as Series Connected Equivalent Resistances or Current Sources

Fig. 2 shows the proposed series connection of propeller drives as simplified equivalent circuit diagram (details on the symbols and underlying assumptions are given below in Sec. III). The DC-link capacitors of each VSC of a voltage level are connected in parallel and thus contribute to a voltage level capacitance. All voltage level capacitances are connected in series. In a simplified consideration, each VSC can be seen either as equivalent resistance (with possibly negative value for generator mode) or as a current source. For a balanced (equal) voltage in each level, the sum of the (paralleled) resistances of each voltage level or the sum of the VSC DC-currents of each voltage level must be equal and equal to the tether current. Note that this does not mean that all equivalent resistances or all VSC DC-currents must be equal.

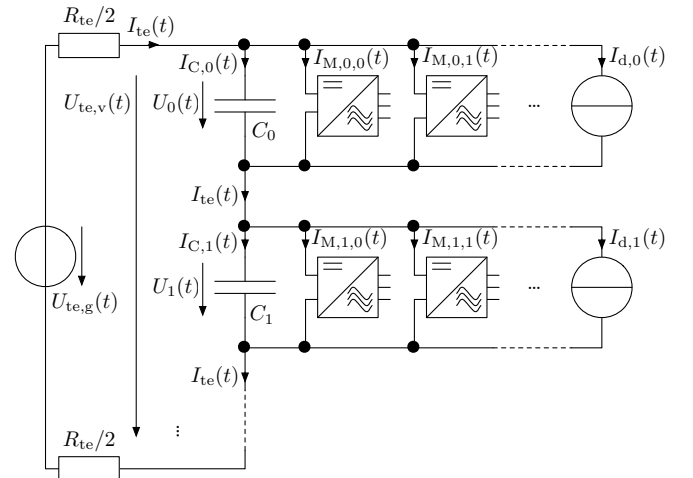


Fig. 2. DC-link model with series connected propeller drives, whereby only the VSC of a drive is drawn. Moreover, a possible disturbance current source in each level is drawn.

### B. Series Connected Switched Loads

Each VSC is a switched load instead of a continuous load. Such switched loads can also be connected in series. The difference to e.g. continuously varying resistances is that the DC-link current of a VSC can step. Consequently, even if the sum of the currents in each voltage level is on average balanced, the voltages are not in general balanced in each instant of time. Instead, the voltages have a ripple due to switching which depends on the current (or power) drawn in each level, the voltage level capacitance, the switching frequency and the phase shift of the pulse width modulation (PWM) of each

VSC. If each PWM has the same frequency and the same phase (i.e. synchronized PWMs), the differential voltage ripple is minimized, because the ripple current of all capacitors are then equal (assuming the powers of all VSCs are approximately equal).

### C. Loads in a Voltage Level for a Drag Power Kite

In addition to propellers, a heater for wing-deicing, servos/hydraulic/pneumatic systems for control surfaces, lights, control computers and sensors may need power onboard a drag power kite. Different possibilities to supply these loads by the tether cables as power source (P) are available:

- (P<sub>1</sub>) Add a high voltage to low voltage (low power) DC-DC-converter at the tether cable terminals on the kite to supply all loads. The disadvantage is the complex and costly high voltage input stage.
- (P<sub>2</sub>) In each voltage level, add an isolated DC-DC-converter (e.g. DAB) and connect each of their output stages in parallel in a new isolated potential. The output voltage can already be quite low (e.g. 48 V) for the possibly low voltage demand of the loads. Consequently, only low voltage semiconductor switches are required for the input and the output stage and all converters might share the same high frequency transformer core.
- (P<sub>3</sub>) Connect all additional loads to one or more voltage levels (only with low voltage DC-DC-converters for the possibly low voltage demand of the loads). The disadvantage would be an almost inevitable intrinsic asymmetry of the power demands of the voltage levels and that some loads are on different potentials (e.g. a micro controller and sensor are on different potentials) unless isolated DC-DC-converters are used.

### D. Voltage Balancing Strategies

The voltages of each level must be stabilized actively, i.e. there must be a possibility to actively increase or decrease the power in each voltage level. Several balancing (B) possibilities are at hand:

- (B<sub>1</sub>) Add additional power electronics to transmit power from any voltage level to any other voltage level. A variety of power electronic topologies may be used e.g. similar circuits which are used for active battery cell balancing, see e.g. [15].
- (B<sub>2</sub>) Use the loads for balancing, e.g. in combination with power source possibility (P<sub>2</sub>) of the last section: If in some voltage levels a high power should be drawn to stabilize the voltages, the loads should be supplied just by these levels. If those DC-DC converters of power source possibility (P<sub>2</sub>) are bidirectional, they can also be used to transmit power from any level to any other level and simultaneously supply the loads in the isolated level.
- (B<sub>3</sub>) Use break resistors (which could also be the heating element in heaters) either in each voltage level as in power source possibility (P<sub>3</sub>), i.e. similar to passive battery cell balancing [15], or in the isolated level of power source possibility (P<sub>2</sub>).

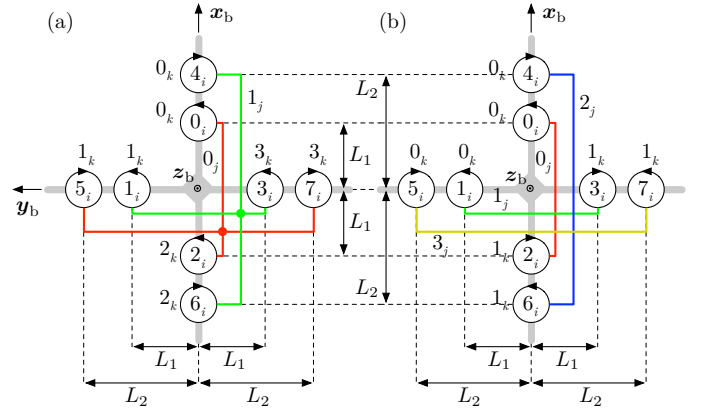


Fig. 3. Octocopter with (a) two series connected quadcopters (SCQs) and (b) four series connected dualcopters (SCDs).

- (B<sub>4</sub>) Control the power factor (i.e. the d-current) of the electrical machines, i.e. reduce the efficiency of the electrical machines.
- (B<sub>5</sub>) Control the power sum of a voltage level while still controlling the overall requested forces and moments of the propellers.

For (B<sub>5</sub>), two meaningful series connection topologies (T) are depicted in Fig. 3 (details on the symbols are given in Sec. III and Tab. I):

- (T<sub>1</sub>) Series connection of quadcopters (SCQ), i.e. each voltage level has four propellers that are placed to form a quadcopter. For voltage balancing, the share of the overall requested propeller forces and moments is varied between each quadcopter and thus between each voltage level. Consequently, the power distribution can be changed to control the voltage of a level, while the overall forces and moments are achieved.
- (T<sub>2</sub>) Series connection of dualcopters (SCD), i.e. each voltage level has two propellers that are placed to form a dualcopter which allows for the same control approach as in (T<sub>1</sub>).

Note that (B<sub>3</sub>) and (B<sub>4</sub>) might be helpful solutions in transient situations, but energy would be wasted and in (B<sub>4</sub>) the maximum torque (or power) of a propeller drive is reduced.

Only the last balancing strategy (B<sub>5</sub>) and multicopter operation (i.e. the propeller drives always draw power, despite transient situations such as braking) are considered in this study. Note that this method has the highest demands on the voltage control algorithm, as it is coupled to the additional control objective to achieve the desired propeller forces and moments. The development of such a control method is in the focus of the remainder of this study.

## III. PROBLEM DESCRIPTION

In the following, a model of the proposed system in Figs. 2 and 3 is derived and the control problem of a multicopter with series connect propeller drives with voltage balancing and simultaneously achieving a desired propeller force sum and propeller moment sum is formulated. Generally, the multicopter is considered to have identical fixed pitch propellers (apart

from rotation direction) at fixed positions and aligned with the vertical vehicle axis pointing upwards. Additional assumptions employed for the mathematical models are highlighted in the text.

Throughout this paper, the following notation is used for iterations:  $m \in \mathbb{N}$  propellers with running index  $i \in [0, m)$ ,  $n \in \mathbb{N}$  voltage levels with running index  $j \in [0, n)$ ,  $o_j \in \mathbb{N}$  propeller drives in voltage level  $j$  with running index  $k \in [0, o_j)$ . Note that propeller drive  $i$  is connected in voltage level  $j$  at position  $k$ , and any value  $x$  of that drive (e.g. voltage, current, propeller speed) can equivalently be indexed by  $x_i$  or  $x_{j,k}$ , i.e. the topology design defines the mapping

$$i = \Gamma(j, k) \quad \text{or} \quad (j, k) = \Gamma^{-1}(i). \quad (1)$$

### A. Voltage Dynamics

Fig. 2 shows the equivalent circuit diagram of the considered DC-link model which implies the following assumptions:

**Assumption 1:** Series inductance, series capacitance and parallel admittance of voltage source and tether are negligible, and can thus be modeled by a series resistance  $R_{te} \in \mathbb{R}_{>0}[\Omega]$  (which is the sum of the series resistance of the ground voltage source and the tether).

**Assumption 2:** Series impedance and parallel admittance of cables onboard the vehicle are negligible.

**Assumption 3:** Series resistance, series inductance and parallel admittance of DC-link capacitors are negligible, and can thus be modeled by the series capacitance  $C_i \in \mathbb{R}_{>0}[\text{F}]$  of drive  $i$ .

Assumptions 1–2 are reasonable as the tether and onboard cables are short for relevant frequencies. Assumption 3 is also a reasonable simplification for DC-link capacitors.

In Fig. 2 the capacitors of one voltage level are summarized to the voltage level capacitance

$$C_j = \sum_{k=0}^{o_j-1} C_{j,k}. \quad (2)$$

The voltage dynamics of each capacitor and thus of each voltage level  $j$  is determined by

$$\dot{U}_j(t) = \frac{1}{C_j} I_{C,j}(t), \quad U_j(t_0) = U_{t_0,j}, \quad (3)$$

where  $I_{C,j}(t) \in \mathbb{R}[\text{A}]$  is the capacitor current at time  $t \in \mathbb{R}[\text{s}]$ ,  $U_j(t) \in \mathbb{R}[\text{V}]$  is the capacitor voltage and  $U_{t_0,j} \in \mathbb{R}[\text{V}]$  is the initial capacitor voltage at initial time  $t_0 \in \mathbb{R}[\text{s}]$ . Employing Kirchhoff's current law, the capacitor current of each voltage level  $j$  is given by

$$I_{C,j}(t) = I_{te}(t) - \sum_{k=0}^{o_j-1} I_{M,j,k}(t) - I_{d,j}(t) \quad (4)$$

where  $I_{te}(t) \in \mathbb{R}[\text{A}]$  is the tether current,  $I_{M,j,k}(t) \in \mathbb{R}[\text{A}]$  is the current drawn by the electrical drive  $k$  in voltage level  $j$  and  $I_{d,j}(t) \in \mathbb{R}[\text{A}]$  is a disturbance current in level  $j$  which models e.g. power consumption of micro controllers or other

(disturbance) loads. Employing Kirchhoff's voltage law, the tether current is given by

$$I_{te}(t) = \frac{U_{te,g}(t) - U_{te,v}(t)}{R_{te}} \quad (5)$$

where  $U_{te,g}(t) \in \mathbb{R}[\text{V}]$  is the tether voltage on ground and  $U_{te,v}(t) \in \mathbb{R}[\text{V}]$  is the tether voltage on the vehicle, which is the sum of the capacitor voltages

$$U_{te,v}(t) = \sum_{j=0}^{n-1} U_j(t). \quad (6)$$

### B. Propeller Aerodynamics

**Assumption 4:** Thrust  $T_i(t) \in \mathbb{R}[\text{N}]$  and torque  $Q_i(t) \in \mathbb{R}[\text{Nm}]$  of propeller  $i$  can be approximated by

$$T_i(t) = k_T \omega_i(t)^2, \quad (7)$$

$$Q_i(t) = k_Q \omega_i(t)^2, \quad (8)$$

where  $\omega_i(t) \in \mathbb{R}_{\geq 0}[\text{rad/s}]$  is the propeller speed and  $k_T \in \mathbb{R}_{> 0}[\text{Ns}^2/\text{rad}]$  and  $k_Q \in \mathbb{R}_{> 0}[\text{Nmms}^2/\text{rad}]$  are constants.

Assumption 4 is reasonable and usually made for multicopters (cf. e.g. [11]–[14] and references therein), because (i) all propellers are identical (except rotation direction) with a fixed pitch, (ii) the air density is approximately constant for approximately constant altitude, (iii) the inflow velocity is approximately zero for low speed flight (hovering), and (iv) the static torque and thrust coefficients are approximately independent of propeller speed or Reynolds number and thus constant.

### C. Propeller Drive

Each propeller is driven by an electrical drive which includes (field-oriented) current-, torque- and speed controllers (cf. e.g. [16] or also [17], [18]). As the inertias of the electrical machine, shaft and propeller are small, the following assumption is made:

**Assumption 5:** The propeller drive inertia  $J_p \in \mathbb{R}_{> 0}[\text{kg m}^2]$  is small compared to vehicle inertias, and thus can be neglected, i.e.  $J_p \approx 0$ . Consequently, the propeller speed control loop is fast compared to the vehicle dynamics, and the demanded reference speed  $\omega_{\text{ref},i}(t) \in \mathbb{R}_{\geq 0}[\text{rad/s}]$  can be considered as actuated instantaneously, i.e.

$$\omega_i(t) \approx \omega_{\text{ref},i}(t). \quad (9)$$

### D. DC-Current of a Propeller Drive

The DC-current of propeller drive  $i$  can be expressed via its electrical power  $P_{M,\text{el},i}(t) \in \mathbb{R}[\text{W}]$  by

$$I_{M,i}(t) = \frac{P_{M,\text{el},i}(t)}{U_i(t)}. \quad (10)$$

The mechanical power  $P_{M,\text{me},i}(t) \in \mathbb{R}[\text{W}]$  of drive  $i$  is with (8) given by

$$P_{M,\text{me},i}(t) = Q_i(t) \omega_i(t) = k_Q \omega_i(t)^3. \quad (11)$$

For simplicity, the following assumption is made:

**Assumption 6:** Losses in the drive are small, so that electrical power  $P_{M,el,i}(t)$  and mechanical power  $P_{M,me,i}(t)$  of propeller drive  $i$  are approximately equal,

$$P_{M,el,i}(t) \approx P_{M,me,i}(t). \quad (12)$$

**Remark 1:** In view of Assumption 6, the (usual) non-minimum phase behavior of DC-link voltage dynamics [19], [20] is neglected. However, as the inductance of the considered electrical machines is very small, this is not critical. If non-minimum phase dynamics were not negligible, model and proposed controllers might need to be extended, e.g. using similar approaches as in [19], [20].

Combining (10)–(12) yields

$$I_{M,i}(t) = \frac{k_Q \omega_i(t)^3}{U_i(t)}. \quad (13)$$

### E. 3D Propeller Forces and Moments on the Vehicle

The thrust exerted by propeller  $i$  adds a force  $\mathbf{F}_{p,i}^b(t) = (F_{p,x,i}^b(t), F_{p,y,i}^b(t), F_{p,z,i}^b(t))^T \in \mathbb{R}^3[\text{N}]$  on the vehicle given by

$$\mathbf{F}_{p,i}^b(t) = \mathbf{e}_M^b T_i(t), \quad (14)$$

where  $\mathbf{e}_M^b = (0, 0, 1)^T$  is the shaft axis unit vector in body coordinates (which is here considered constant and parallel to the vertical vehicle axis).

As the propellers are mounted with a lever arm to the center of mass  $\mathbf{r}_{p,i}^b = (r_{p,x,i}^b, r_{p,y,i}^b, r_{p,z,i}^b)^T \in \mathbb{R}^3[\text{m}]$ , the thrust of propeller  $i$  also adds a moment

$$\mathbf{M}_{p,i}^b(t) = \mathbf{r}_{p,i}^b \times \mathbf{F}_{p,i}^b(t). \quad (15)$$

The electrical machine “pushes” the propeller in one angular direction and consequently the vehicle is “pushed” in the opposite angular direction. With Assumption 5 the torque of the electrical machine is the same as the propeller torque. Consequently, each machine also adds the moment

$$\mathbf{M}_{M,i}^b(t) = -\sigma_i \mathbf{e}_M^b Q_i(t), \quad (16)$$

where  $\sigma_i \in \{+1, -1\}$  is the rotation direction of propeller  $i$  with  $\sigma_i = +1$  for counter-clockwise (propeller seen from top) and  $\sigma_i = -1$  for clockwise.

Each propeller shaft also contributes a gyroscopic effect, which is however neglected through Assumption 5.

Combining (7)–(8) with (14)–(16) yields

$$\boldsymbol{\tau}(t) = \mathbf{H} \boldsymbol{\delta}(t) \quad (17)$$

where

$$\boldsymbol{\tau}(t) = \left( F_{p,\Sigma,z}^b(t), M_{p,\Sigma,x}^b(t), M_{p,\Sigma,y}^b(t), M_{p,\Sigma,z}^b(t) \right)^T, \quad (18)$$

is the virtual control vector,

$$\mathbf{H} = \begin{pmatrix} k_T & k_T & \dots & k_T \\ r_{p,y,0}^b k_T & r_{p,y,1}^b k_T & \dots & r_{p,y,m-1}^b k_T \\ -r_{p,x,0}^b k_T & -r_{p,x,1}^b k_T & \dots & -r_{p,x,m-1}^b k_T \\ -\sigma_0 k_Q & -\sigma_1 k_Q & \dots & -\sigma_{m-1} k_Q \end{pmatrix} \quad (19)$$

is the control effectiveness matrix, and

$$\boldsymbol{\delta}(t) = \left( \omega_0(t)^2, \omega_1(t)^2, \dots, \omega_{m-1}(t)^2 \right)^T \quad (20)$$

is the control vector (cf. e.g. [11]–[14] and references therein).

### F. Control Problem Formulation

The control problem can be formulated as follows: Find a control algorithm that simultaneously stabilizes the voltages in each level and generates a desired virtual control vector, i.e.

$$\lim_{t \rightarrow \infty} \left( \boldsymbol{\tau}_{\text{ref}}(t) - \boldsymbol{\tau}(t) \right) \approx 0 \quad (21)$$

$$\lim_{t \rightarrow \infty} \left( U_{\text{ref},j}(t) - U_j(t) \right) \approx 0 \quad (22)$$

with  $U_{\text{ref},j}(t) = r_j(t) U_{\text{te},v}(t)$ ,  $\sum_{j=0}^{n-1} r_j(t) = 1$ ,  $r_j(t) \in (0, 1]$ , where  $U_{\text{ref},j}(t)$  is the voltage reference of level  $j$  and  $\boldsymbol{\tau}_{\text{ref}}(t)$  is the virtual control vector reference. The control algorithm shall be simple for reduced debugging and tuning efforts as well as for reduced hardware performance demands (low cost micro controllers and communication busses).

## IV. PROPOSED SOLUTION

Fig. 4 shows the block diagram of the proposed control method, which is derived in the following.

### A. Multicopter Control

To solve the control problem (21)–(22), a conventional cascaded multicopter controller with inversion based control allocation is adopted (cf. e.g. [11]–[14] and references therein), and then extended by a voltage stabilization: The inner most controllers consist of the AC-motor current controllers, torque controllers and propeller speed controllers. These controllers are already idealized by Assumption 5 and are executed independently on each ESC. The next superimposed controller is an inversion-based control allocation given with (17) and Assumption 5 by

$$\boldsymbol{\delta}_{\text{ref}}(t) = \text{inv}(\mathbf{H}) \boldsymbol{\tau}_{\text{ref}}(t), \quad (23)$$

where  $\boldsymbol{\delta}_{\text{ref}}(t)$  contains the squares of the propeller speed references, and

$$\text{inv}(\mathbf{H}) = \mathbf{H}^T \left( \mathbf{H} \mathbf{H}^T \right)^{-1} \quad (24)$$

is the pseudo inverse (which is constant and can be solved offline). As  $0 \leq \underline{\omega}_i(t) \leq \omega_{\text{ref},i}(t) \leq \bar{\omega}_i(t)$ , a clipping is applied and the reference propeller speeds are

$$\omega_{\text{ref},i} = \begin{cases} \underline{\omega}_i(t) & \text{for } \delta_{\text{ref},i}(t) \leq \underline{\omega}_i(t)^2 \\ \bar{\omega}_i(t) & \text{for } \delta_{\text{ref},i}(t) \geq \bar{\omega}_i(t)^2 \\ \sqrt{\delta_{\text{ref},i}(t)} & \text{otherwise} \end{cases} \quad (25)$$

where  $\delta_{\text{ref},i}(t)$  is the  $i$ th component of vector  $\boldsymbol{\delta}_{\text{ref}}(t)$ . With (23)–(25) the first part of the control problem (21) is achieved (if no clipping (25) is required).

Note that  $\boldsymbol{\tau}_{\text{ref}}(t)$  is the output of superimposed controllers, such as attitude and position controllers. The control allocation and those superimposed controllers are executed on a central micro controller, see Fig. 4.

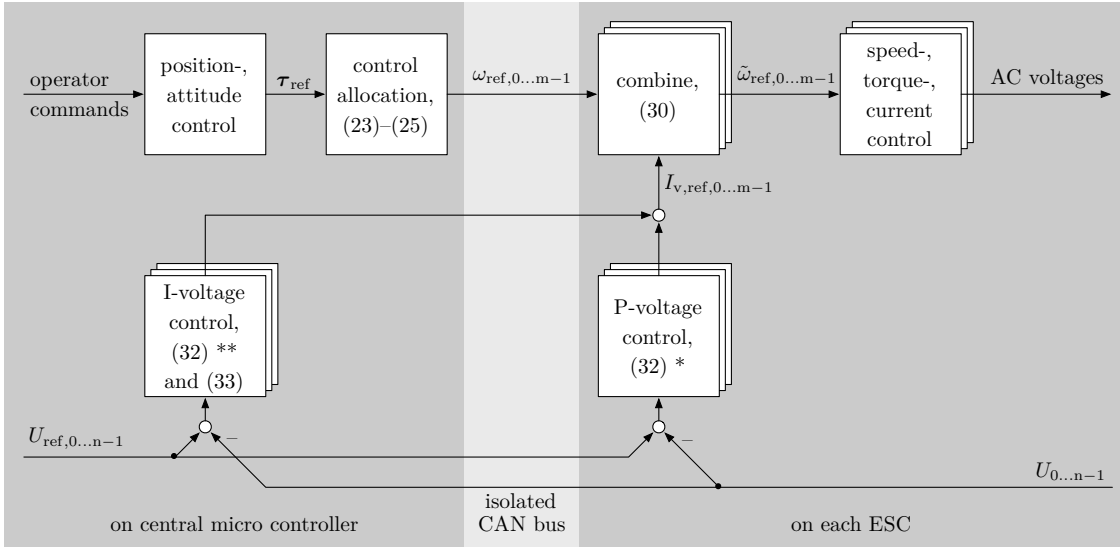


Fig. 4. Block diagram of the proposed control method.

### B. Voltage Control via Propeller Speed Offset (or via Virtual Control Current)

For a simple voltage control approach, only “symmetric” topologies such as SCQ and SCD mentioned in Sec. II-D and shown in Fig. 3 are considered: If the voltage of a level is above its reference voltage, the powers of all propellers of that level are increased, i.e. the propeller speeds are increased, and vice versa if the voltage of a level is below its reference voltage. As the propellers in such symmetric topologies are placed so that their torques and moments cancel out, mainly the thrust of that copter is increased. Since at the same time the voltage of another copter would be below its reference, the thrust of that copter would be decreased approximately by the same amount. As a consequence, such symmetric topologies allow to impose the following assumption:

**Assumption 7:** *Differential propeller speed offsets in the different voltage levels hardly affect  $\tau(t)$ .*

With Assumption 7, the propeller speed reference is modified to

$$\tilde{\omega}_{ref,i}(t) = \omega_{ref,i}(t) + v_i(t) \quad (26)$$

with  $\omega_{ref,i}(t)$  from (23)–(25) and offset  $v_i(t) \in \mathbb{R}[\text{rad/s}]$ . This offset alters the resulting drive DC-current, given by inserting (26) into (13) with Assumption 5

$$\tilde{I}_{M,i}(t) = \frac{k_Q}{U_i(t)} \left( \omega_i(t) + v_i(t) \right)^3. \quad (27)$$

The difference between  $\tilde{I}_{M,i}(t)$  and  $I_{M,i}(t)$  is

$$I_{V,i}(t) = \tilde{I}_{M,i}(t) - I_{M,i}(t) \quad (28)$$

$$= \frac{k_Q}{U_i(t)} \left[ \left( \omega_i(t) + v_i(t) \right)^3 - \omega_i(t)^3 \right]. \quad (29)$$

The idea is to find an expression for  $v_i(t)$  which yields a desired current  $I_{V,i}(t)$ , i.e. to interpret  $I_{V,i}(t)$  as virtual control input.

That expression is found by solving (29) for  $v_i(t)$  and inserting the result into (26), which, with Assumption 5, becomes

$$\tilde{\omega}_{ref,i}(t) = \sqrt[3]{\omega_{ref,i}(t)^3 + \frac{U_i(t)}{k_Q} I_{V,ref,i}(t)}, \quad (30)$$

where  $I_{V,ref,i}(t)$  is the reference of the offset current. This reference generation (30) divides each propeller drive  $i$  into an uncontrolled current source (disturbance) caused by  $\omega_{ref,i}$  (first term in (30)), and a controlled current source  $I_{V,ref,i}(t)$  (second term in (30)), with which the voltages can be stabilized. Note that the latter term of the radicand with  $I_{V,ref,i}(t)$  becomes less dominant for increasing  $\omega_{ref,i}(t)$ , and if  $I_{V,ref,i}(t) = 0$  then  $\tilde{\omega}_{ref,i}(t) = \omega_{ref,i}(t)$ . Consequently, the reference speed and thus force, torque and power of propeller  $i$  are only changed if there is a requested control current. Moreover, to fulfill the condition  $\tilde{\omega}_{ref,i}(t) \geq \omega_i(t) \geq 0$ , the offset current reference must be limited by the lower bound

$$I_{V,ref,i}(t) \geq \underline{I}_{V,ref,i}(t) = \frac{k_Q}{U_j(t)} \left( \omega_i(t)^3 - \omega_{ref,i}(t)^3 \right). \quad (31)$$

For propeller drive  $i$  which is connected to voltage level  $j$  at position  $k$  (cf. (1)), the PI-voltage controllers

$$I_{V,ref,j,k}(t) = \underbrace{K_{P,j,k} \left( U_{ref,j}(t) - U_j(t) \right)}_{*} + \underbrace{K_{I,j,k} \zeta_j(t)}_{**} \quad (32)$$

$$\dot{\zeta}_j(t) = U_{ref,j}(t) - U_j(t), \quad \zeta_j(t_0) = \zeta_{t_0,j}(t) \quad (33)$$

are proposed, where  $K_{P,j,k} \in \mathbb{R}[A/V]$  and  $K_{I,j,k} \in \mathbb{R}[A/(Vs)]$  are proportional and integral gains and  $\zeta_j(t) \in \mathbb{R}[Vs]$  is the integral of the voltage error of level  $j$ . Note that the part highlighted by \* can be executed on each ESC individually with the same high control cycle frequency (and thus response time) as the speed controller (considering that  $U_{ref,j}(t) \approx \text{const.}$  and  $U_{j,k}(t) \approx U_j(t)$  is measured locally), whereas the part highlighted by \*\* and (33) can be executed on a central micro controller. This control method is inspired by the frequency (or power) control of the power system with primary control

(local P-controller in the power plants, here on the ESC) and secondary control (global I-controller by the grid operator, here on the central micro controller). Consequently, a runaway of the integrators due to measurement offsets is avoided, which would occur if a PI-controller was executed on each ESC.

It can be shown, that P-controllers, i.e. (32) where the part \*\* is dropped (set to zero), can stabilize the voltages:

**Theorem 1 (Stability of P-Voltage Control):** Consider the circuit in Fig. 2 with (2)–(6), (13), (30), where each voltage level has bounded loads (disturbances) and at least one controllable current source  $I_{v,\text{ref},j,k}$  (inputs). Consider the voltage controller (32) where the part \*\* is dropped (i.e.  $K_{I,j,k} = 0$ ). Consider further  $\forall j : C_j = C, \sum_{k=0}^{o_j-1} K_{P,j,k} = K_P$ . Then the closed-loop system is stable if

$$K_P < 0. \quad (34)$$

*Proof.* See appendix.

However, a steady-state disturbance current (power) leads to a steady-state voltage error if just P-controllers are used. It can be shown that PI-controllers, i.e. (32)–(33), can also stabilize the voltages, without steady-state error under steady-state disturbances:

**Theorem 2 (Stability of PI-Voltage Control):** Consider the circuit in Fig. 2 with (2)–(6), (13), (30), where each voltage level has bounded loads (disturbances) and at least one controllable current source  $I_{v,\text{ref},j,k}$  (inputs). Consider the voltage controller (32)–(33). Consider further  $\forall j : C_j = C, \sum_{k=0}^{o_j-1} K_{P,j,k} = K_P, \sum_{k=0}^{o_j-1} K_{I,j,k} = K_I$ . Then the closed-loop system is stable if

$$-\frac{n}{R_{\text{te}}} \leq K_P < 0 \quad \wedge \quad \frac{K_P n}{C R_{\text{te}}} \leq K_I < 0 \quad (35)$$

or

$$K_P < -\frac{n}{R_{\text{te}}} < 0 \quad \wedge \quad K_I \leq -\frac{(R_{\text{te}} K_P - n)^2}{C R_{\text{te}}^2} < 0. \quad (36)$$

*Proof.* See appendix.

### C. Influence of the Voltage Control on the Control Vector: Discussion of Assumption 7

Assumption 7 holds true only if  $I_{v,\text{ref},i}(t)$  is small,  $\omega_{\text{ref},i}$  is high, and/or the voltage error is small  $U_j(t) \approx U_{\text{ref},j}(t)$ , cf. (30). Moreover, the influence of the voltage control is minimized, if an equal increase of the propeller speeds in any voltage level hardly affects  $\tau(t)$ , which can be seen as fulfilled for symmetric topologies such as SCQ and SCD (see Fig. 3). However, because  $T_i(t), Q_i(t) \sim \omega_i(t)^2$  (cf. (7)–(8)) whereas the voltage control adds  $\Delta\omega_i(t)^3 \sim I_{v,\text{ref},i}(t)$  (cf. (30)), the voltage control does affect  $\tau(t)$ : The error is  $\Delta\tau(t) = \tau_{\text{ref}}(t) - \tilde{\tau}_{\text{ref}}(t)$  where  $\tilde{\tau}_{\text{ref}}(t)$  results from (23)–(33). Fig. 5 plots the errors of the force sum and the roll moment for the topology in Fig. 3 (a) and  $\Delta U(t) = U_{\text{ref},0}(t) - U_0(t) = -U_{\text{ref},1}(t) + U_1(t) \in [-2\text{ V}, 2\text{ V}]$ ,  $U_{\text{ref},0}(t) = U_{\text{ref},1}(t) = 24\text{ V}$ ,  $\zeta_0(t) = \zeta_1(t) = 0$  and otherwise the data in Tab. I. Note that, at  $|\Delta U(t)| = 2\text{ V}$ , the propeller power difference between the two voltage levels is already  $|\sum_{k=0}^3 I_{v,\text{ref},0,k}(t)U_0(t) - \sum_{k=0}^3 I_{v,\text{ref},1,k}(t)U_1(t)| = 192\text{ W}$ , while the rated power of

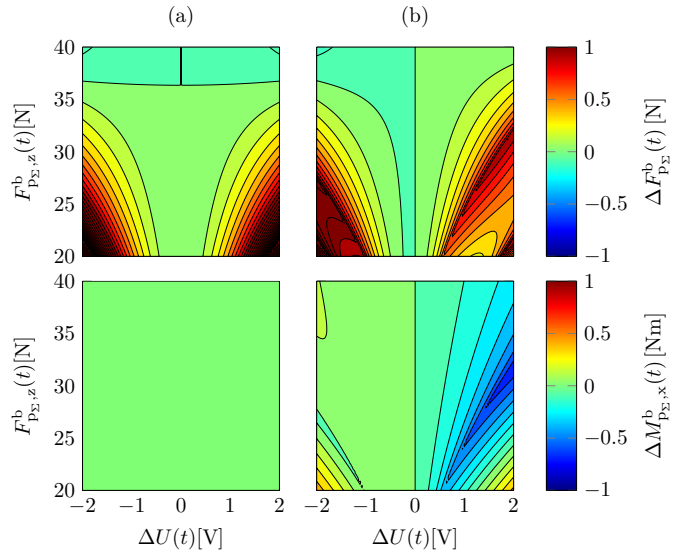


Fig. 5. Error of propeller force sum  $\Delta F_{P_{\Sigma,z}}^b(t)$  (top) and of propeller roll moment sum  $\Delta M_{P_{\Sigma,x}}^b(t)$  (bottom) through voltage control for  $\tau_{\text{ref}}(t) \in \{(20 \dots 40\text{ N}, 0, 0, 0)^T\}$  (a) or  $\tau_{\text{ref}}(t) \in \{(20 \dots 40\text{ N}, 2\text{ Nm}, 0, 0)^T\}$  (b).

one propeller drive is only  $\approx 100\text{ W}$ . Yet, the error  $\Delta\tau(t)$  is (almost) negligible for a relevant force  $F_{P_{\Sigma,z}}^b(t) \approx 30 \dots 40\text{ N}$ . The results are similar for the topology in Fig. 3 (b) (not shown in Fig. 5). Consequently, Assumption 7 can be confirmed, particularly for high  $\omega_i(t)$  and low  $I_{v,\text{ref},i}(t)$ .

## V. IMPLEMENTATION AND EXPERIMENTAL RESULTS

### A. Setup

The proposed series connections and control method were tested with an octocopter demonstrator shown in Fig. 6 and 7. The vehicle was tethered to a ground station with ground tether angle sensors, which consisted of potentiometers and rods and were designed similar to the angle sensors of [21]. With the angle sensors, the vehicle's elevation and azimuth positions were reconstructed and hence, with the knowledge of the fixed tether length, the vehicle's position was available in spherical coordinates for position control (which includes altitude control). The tether bridles consisted of “three Y”-connections (cf. Fig. 7) which constrained the vehicle's yaw angle, similar to [4].

The propellers had 10 in diameter and “5 in pitch”. The motors were three-phase BLDC (or permanent magnet) machines and were controlled with custom-built VSCs (ESCs) with 6...60 V DC-link voltage range. On each ESC field oriented current control, torque control, speed control and the P-part of the voltage control (cf. Fig. 4) were executed with 10 kHz control cycle frequency and 20 kHz PWM frequency. All ESCs communicated via an isolated CAN bus, which was the only “special” design consideration for a possible series connection, with which any of the ESCs could be connected to any voltage level. Each ESC measured its DC-link voltage based on a voltage divider, which was calibrated (by software) before flight. Each ESC used its DC voltage reading for the P-Voltage control.

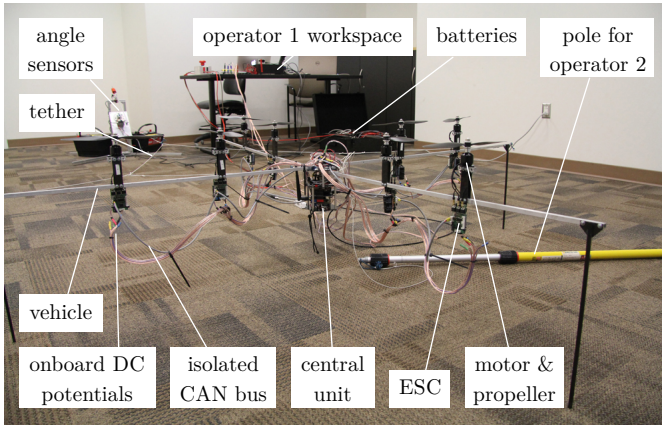


Fig. 6. Experimental setup of the demonstrator with 2 m span.

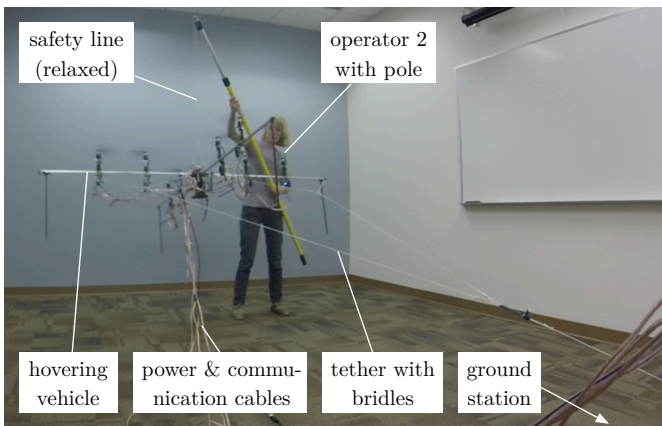


Fig. 7. Demonstrator during test flight. (The safety line of the pole of operator 2 is relaxed during normal operation. The only task of operator 2 is to rescue the vehicle in case of unexpected behavior, for which operator 1 would shut down the tether voltage.)

A low cost central micro controller in the center of mass of the vehicle was connected to the CAN bus. Additional sensors such as an inertial measurement unit and communication interfaces for operator commands and monitoring were connected to the central micro controller. The central micro controller executed the I-part of the voltage control, the control allocation and superimposed controllers, such as attitude and position controllers (cf. Fig. 4), with 100 Hz control cycle frequency. Each voltage of a voltage level for the I-controller was reconstructed as the average of all measured voltages of all ESCs of the respective voltage level.

All voltage levels of the vehicle were conducted to the ground by cables to additionally measure the voltages e.g. with a multimeter during flight and to induce an additional disturbance to challenge the voltage controller. The power supply was a stack of four series connected 12 V lead-acid batteries on the ground connected to the vehicle via a two-phase cable. During the flight tests, a first operator (operator 1) monitored and turned on and off the system while a second operator (operator 2) held a pole, which was connected to the vehicle by a rope (safety line), see Fig. 7: In case of an unexpected behavior, operator 1 would shut down the tether

TABLE I  
RELEVANT DEMONSTRATOR PARAMETERS (SEE ALSO FIG. 3).

| Parameter                        | Symbol & Value   |
|----------------------------------|--|
| arm lengths                      | $(L_1, L_2) = (0.325 \text{ m}, 0.590 \text{ m})$  |
| propeller constants              | $k_T \approx 1.52 \cdot 10^{-5} \text{ N s}^2/\text{rad}$<br>$k_Q \approx 2.95 \cdot 10^{-7} \text{ N m s}^2/\text{rad}$ |
| tether voltage on ground         | $U_{te,g}(t) \approx 48 \text{ V}$   |
| power supply & tether resistance | $R_{te} \approx 0.6 \Omega$  |
| VSC DC-capacitor                 | $\forall i : C_i = 2.2 \text{ mF}$   |
| voltage reference ratio          | $\forall j, t : r_j(t) = 1/n$  |
| P-gain                           | $\forall j, k : K_{P,j,k} = -0.5 \text{ A/V}$  |
| I-gain                           | $\forall j, k : K_{I,j,k} = -5 \text{ A/(Vs)}$   |

voltage, and operator 2 would catch/rescue the vehicle. As highlighted in Fig. 7, the safety line of the pole of operator 2 was relaxed during normal flight operation.

The control algorithm was implemented in C++. Before experimental testings, the system was simulated with a detailed model implemented in C++. Tab. I lists relevant demonstrator parameters.

### B. Experiments

The vehicle was hovered on the tether at an almost constant position with a pitch angle of  $\theta_{ref}(t) = 10^\circ$  so that the tether was under tension for an effective position measurement with the tether angle sensors. The two topologies in Fig. 3 either with P- or PI-voltage controllers and, as reference-scenario, also a pure parallel connection were tested.

Fig. 8 shows the recorded measurements: In all cases, the vehicle flew stably for several minutes, until the test was terminated by the operators.<sup>2</sup> Additionally, at time  $t_s \in \mathbb{R}[s]$ , the reference pitch angle was changed to  $\theta_{ref}(t) = 20^\circ$  (i.e. reference step response) and about  $2 \dots 3 \text{ s}$  later a  $R_d = 15 \Omega$  resistor was added to voltage level  $j = 0$  and thus a defined disturbance current was added (i.e. disturbance step response). The proposed control method stabilized the voltages and achieved the desired control vector  $\tau_{ref}(t)$ , i.e. the control problem (22)–(21) was solved successfully. The controllers also stabilized the attitude as well as position of the vehicle. The control error for all control variables was small. Only the control error of the azimuth angle appears large compared to the other angles, which however can be explained by the chosen relatively slow closed-loop time constant of the azimuth angle controller. No considerable difference between the investigated drive connections was visible in the vehicle dynamics (cf. the first five diagrams of Fig. 8 (a)–(e)). The noise of the measurements was mainly caused by the low resolution of the data transmission and estimators of the propeller speeds, which were used to compute the propeller force sum and moment sums with (17). The voltage errors were at all times less than  $\forall j : |\Delta U_j(t)| < 0.75 \text{ V}$  and the P-controller had a steady-state error while the PI-controller had not, as expected. Note that no voltage control was necessary for the pure parallel

<sup>2</sup>The longest flight in the records was a bit more than three minutes. That particular test and the ones shown in Fig. 8 were terminated by the operators when the anticipated measurements were obtained. However, much longer flight times could have been possible, maybe for hours, until the ground station batteries were empty.

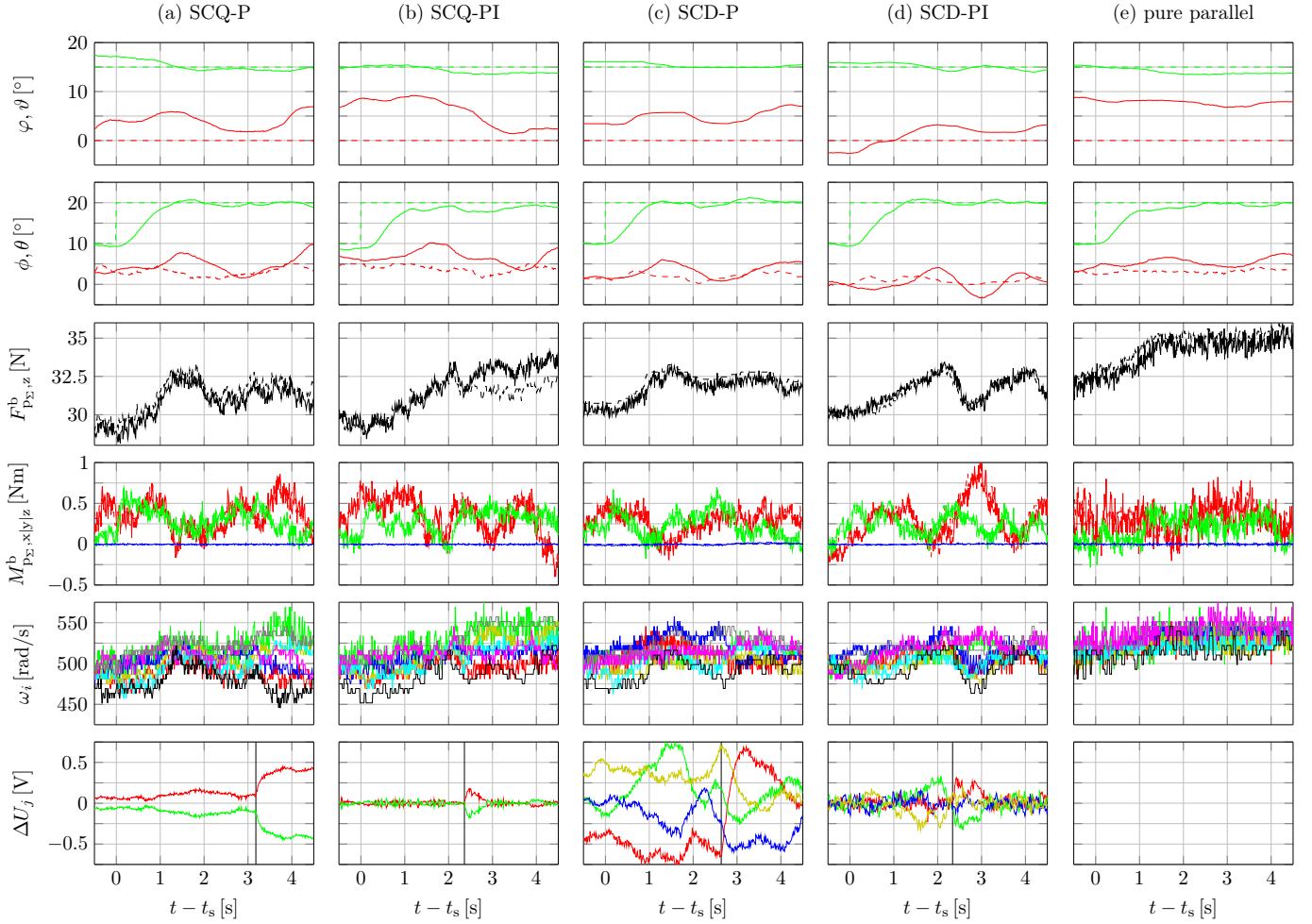


Fig. 8. Recorded measurements for the topologies SCQ with (a) P- and (b) PI-voltage controllers respectively, SCD with (c) P- and (d) PI-voltage controllers respectively, and (e) for a pure parallel connection of all propeller drives as reference-scenario. From top to bottom azimuth  $\varphi$  (—) and elevation  $\vartheta$  (—) angles; roll  $\phi$  (—) and pitch  $\theta$  (—) angles; propeller force sum  $F_{p_{\Sigma,z}}^b$  (—); propeller moment sums  $M_{p_{\Sigma,x}}^b(t)$  (—),  $M_{p_{\Sigma,y}}^b(t)$  (—) and  $M_{p_{\Sigma,z}}^b(t)$  (—); propeller speeds  $\omega_0$  (—),  $\omega_1$  (—),  $\omega_2$  (—),  $\omega_3$  (—),  $\omega_4$  (—),  $\omega_5$  (—),  $\omega_6$  (—) and  $\omega_7$  (—); and voltage errors  $\Delta U_j(t) = U_{\text{ref},j}(t) - U_j(t)$  with  $\Delta U_0$  (—),  $\Delta U_1$  (—),  $\Delta U_2$  (—), and  $\Delta U_3$  (—). In all plots, measured (or estimated/filtered) values are solid lines (—) while demanded values are dashed lines (---). At time  $t = t_s$  the pitch angle reference was changed from  $\theta_{\text{ref}}(t) = 10^\circ$  to  $20^\circ$  and about 2...3 s later a  $R_d = 15 \Omega$  resistor was added in voltage level  $j = 0$ , indicated by a vertical black line in the bottom plots.

connection which is why the bottom plot of Fig. 8 (e) contains no data. However, this case is actually also covered by the proposed general formulation of the voltage controller: As  $n = 1$  and  $U_{\text{te},v}(t) = U_0(t)$ , the voltage error of the first level is always  $\Delta U_0(t) = U_{\text{ref},0}(t) - U_0(t) = r_0(t)U_{\text{te},v}(t) - U_{\text{te},v}(t) = \frac{1}{1}U_{\text{te},v}(t) - U_{\text{te},v}(t) = 0$ , hence always  $\forall i, j: I_{v,\text{ref},j,k}(t) = 0$ . The measurement results matched with the simulation results of a detailed system model (not presented here) and to the theoretical results in terms of stability and attenuation according to (49) and (54), respectively.

It should be noted, that the purpose of the built demonstrator and the test flights was a proof-of-principle. An actual application such as crosswind kite power requires a tether voltage in the order of 10 kV, which is several magnitudes higher than the used 48 V. However, with such a low voltage, it was possible to quickly build and test-fly a cost-efficient demonstrator without the dangers imposed by high voltages. Moreover, a stability proof for the general case is given in the appendix.

## VI. CONCLUSIONS AND OUTLOOK

This study proposed to connect propeller drives of a tethered multicopter partly in series to divide a possibly high tether voltage into smaller voltages for each propeller drive. Hence, additional DC-DC-power converter design and mass can be avoided. A control method to stabilize the voltage of each level while generating the requested propeller forces and moments was developed: Besides using the additional degrees of freedom given through a high number of propellers  $n \gg 4$ , the key ideas were (i) conventional multicopter control, (ii) “symmetric” choice of the propellers in the voltage levels such as series connected quadcopters or series connected dualcopters, and thus create the possibility to increase the power of any quadcopter (dualcopter) and simultaneously decrease the power of other quadcopters (dualcopters) to stabilize the voltages without (or hardly) affecting the total forces and moments, (iii) increase (decrease) of propeller speeds of a voltage level if its voltage is too high (low), (iv) inversion of the nonlinear equations of

the propeller power so that one propeller drive is thought as combination of a controlled current source and a disturbance, and (v) linear PI-controllers to control the linear electrical system, that is decoupled from the propeller-generated vehicle forces and moments through steps (ii)–(iv). Theoretical, numerical and experimental validations demonstrated the feasibility of the approach. The proposed control method was effective in achieving reference tracking of forces and moments while suppressing disturbances in the voltage levels.

Future works will focus on a formal approach of feasible geometrical and electrical propeller placements, fault-tolerant control, crosswind flight with power generation (crosswind kite power/drag power), higher tether voltages, and improved control methods (e.g. Nonlinear Model Predictive Control). With the latter some assumptions made in this study could be abandoned and thus e.g. extend the controller to be applicable also in crosswind flights for power generating kites.

## APPENDIX

### PROOF OF THEOREM 1: STABILITY OF P-VOLTAGE CONTROL

The system (3)–(17), (23)–(30) with the P-voltage controllers (32), where the part \*\* is dropped ( $K_{I,j,k} = 0$ ), can be written as

$$\dot{\mathbf{x}}(t) = \mathbf{f}_{c,p}(\mathbf{x}(t), \mathbf{u}_1(t), \mathbf{u}_c(t)), \quad \mathbf{x}(t_0) = \mathbf{x}_{t_0} \quad (37)$$

with closed-loop system state vector

$$\begin{aligned} \mathbf{x}(t) &= (x_0(t), x_1(t), \dots, x_{n-1}(t))^\top \\ &= (U_0(t), U_1(t), \dots, U_{n-1}(t))^\top, \end{aligned} \quad (38)$$

closed-loop control inputs

$$\begin{aligned} \mathbf{u}_1(t) &= (u_{1,0}(t), u_{1,1}(t), \dots, u_{1,m-1}(t))^\top \\ &= (\omega_{\text{ref},0,0}(t), \omega_{\text{ref},0,1}(t), \dots, \omega_{\text{ref},0,o_0-1}(t), \\ &\quad \omega_{\text{ref},1,0}(t), \omega_{\text{ref},1,1}(t), \dots, \omega_{\text{ref},1,o_1-1}(t), \\ &\quad \dots, \omega_{\text{ref},n-1,o_{n-1}-1}(t))^\top \end{aligned} \quad (39)$$

$$\mathbf{u}_c(t) = (U_{\text{ref},0}(t), U_{\text{ref},1}(t), \dots, U_{\text{ref},n-1}(t))^\top, \quad (40)$$

closed-loop system function

$$\begin{aligned} \mathbf{f}_{c,p}(\mathbf{x}(t), \mathbf{u}_1(t), \mathbf{u}_c(t)) &= \mathbf{A}_{c,p}\mathbf{x}(t) + \mathbf{B}_{c,p}\mathbf{u}_c(t) \\ &\quad + \mathbf{d}(\mathbf{x}(t), \mathbf{u}_1(t), t), \end{aligned} \quad (41)$$

closed-loop system matrix

$$\mathbf{A}_{c,p} = \begin{pmatrix} \frac{R_{te}K_{P,0}-1}{R_{te}C_0} & -\frac{1}{R_{te}C_0} & \cdots & -\frac{1}{R_{te}C_0} \\ -\frac{1}{R_{te}C_1} & \frac{R_{te}K_{P,1}-1}{R_{te}C_1} & \cdots & -\frac{1}{R_{te}C_1} \\ \vdots & \vdots & \ddots & \vdots \\ -\frac{1}{R_{te}C_{n-1}} & -\frac{1}{R_{te}C_{n-1}} & \cdots & \frac{R_{te}K_{P,n-1}-1}{R_{te}C_{n-1}} \end{pmatrix}, \quad (42)$$

closed-loop input matrix

$$\mathbf{B}_{c,p} = \begin{pmatrix} -\frac{K_{P,0}}{C_0} & 0 & \cdots & 0 \\ 0 & -\frac{K_{P,1}}{C_1} & \cdots & 0 \\ \vdots & \vdots & \ddots & \vdots \\ 0 & 0 & \cdots & -\frac{K_{P,n-1}}{C_{n-1}} \end{pmatrix}, \quad (43)$$

and closed-loop disturbance function

$$\begin{aligned} \mathbf{d}(\mathbf{x}(t), \mathbf{u}_1(t), t) &= \begin{pmatrix} -\frac{k_Q}{C_0} \frac{1}{x_0(t)} \sum_{k=0}^{o_0-1} \omega_{\text{ref},0,k}(t)^3 \\ -\frac{k_Q}{C_1} \frac{1}{x_1(t)} \sum_{k=0}^{o_1-1} \omega_{\text{ref},1,k}(t)^3 \\ \vdots \\ -\frac{k_Q}{C_{n-1}} \frac{1}{x_{n-1}(t)} \sum_{k=0}^{o_{n-1}-1} \omega_{\text{ref},n-1,k}(t)^3 \end{pmatrix} \\ &\quad + \begin{pmatrix} \frac{1}{C_0 R_{te}} U_{te,g}(t) - \frac{1}{C_0} I_{d,0}(t) \\ \frac{1}{C_1 R_{te}} U_{te,g}(t) - \frac{1}{C_1} I_{d,1}(t) \\ \vdots \\ \frac{1}{C_{n-1} R_{te}} U_{te,g}(t) - \frac{1}{C_{n-1}} I_{d,n-1}(t) \end{pmatrix}, \end{aligned} \quad (44)$$

where

$$K_{P,j} := \sum_{k=0}^{o_j-1} K_{P,j,k} \quad (45)$$

was summarized (without loss of generality). Note that the inputs  $\mathbf{u}_1(t)$  to generate the desired control vector  $\boldsymbol{\tau}_{\text{ref}}(t)$  (cf. (23)–(26)) are interpreted as disturbance. The system is stable, if the real parts of all eigenvalues of  $\mathbf{A}_{c,p}$  are negative, and if the disturbance  $\mathbf{d}(\mathbf{x}(t), \mathbf{u}_1(t), t)$  is bounded.

**Remark 2:** In each row  $j$  of  $\mathbf{d}(\mathbf{x}(t), \mathbf{u}_1(t), t)$  is a state dependent term

$$\frac{k_Q}{C_j} \frac{1}{x_j(t)} \sum_{k=0}^{o_j-1} \omega_{\text{ref},j,k}(t)^3 \quad (46)$$

(cf. (44)) which is not in general bounded, e.g. for  $x_j(t) \rightarrow 0$  and  $\sum_{k=0}^{o_j-1} \omega_{\text{ref},j,k}(t)^3 \neq 0$ . However, the disturbance can be bounded by saturating the speed references  $\omega_{\text{ref},j,k}(t)$  as function of the state in the controller. A possible implementation is

$$\omega'_{\text{ref},j,k}(t) = \begin{cases} \sqrt[3]{\frac{x_j(t)}{x_{th,j}(t)}} \omega_{\text{ref},j,k}(t) & \text{for } x_j(t) < x_{th,j}(t) \\ \omega_{\text{ref},j,k}(t) & \text{otherwise} \end{cases} \quad (47)$$

where  $\omega'_{\text{ref},j,k}(t)$  is the saturated speed reference and  $x_{th,j}(t) > 0$  is a (possibly constant) threshold. Consequently, if  $x_j(t) < x_{th,j}(t)$ , (46) becomes

$$\frac{k_Q}{C_j} \frac{1}{x_{th,j}(t)} \sum_{k=0}^{o_j-1} \omega_{\text{ref},j,k}(t)^3 \quad (48)$$

which is bounded, and not a function of a state.

A simple analytical solution of the eigenvalues was found using Matlab's Symbolic Toolbox for the special (but meaningful) case  $\forall j: C_j = C, K_{P,j} = K_P$  for which the  $n$  eigenvalues of  $\mathbf{A}_{c,p}$  become

$$\left. \begin{aligned} \lambda_0 &= \frac{R_{te}K_P - n}{R_{te}C} \\ \text{for } n > 1, \forall j < n: \lambda_j &= \frac{K_P}{C}. \end{aligned} \right\} \quad (49)$$

Obviously, if  $K_P < 0$  then  $\forall j: \Re\{\lambda_j\} < 0$  and the system is stable. ■

PROOF OF THEOREM 2: STABILITY OF PI-VOLTAGE CONTROL

With the voltage controller (32)–(33), the system function (41) becomes

$$\begin{aligned} \mathbf{f}_{c,PI}(\tilde{\mathbf{x}}(t), \mathbf{u}_1(t), \mathbf{u}_c(t)) &= \mathbf{A}_{c,PI}\tilde{\mathbf{x}}(t) + \begin{pmatrix} \mathbf{B}_{c,P} \\ \mathbf{0}_{n \times n} \end{pmatrix} \mathbf{u}_c(t) \\ &\quad + \begin{pmatrix} \mathbf{I}_n \\ \mathbf{0}_{n \times n} \end{pmatrix} \mathbf{d}(\mathbf{x}(t), \mathbf{u}_1(t), t) \end{aligned} \quad (50)$$

with closed-loop system matrix and closed-loop state vector

$$\mathbf{A}_{c,PI} = \begin{pmatrix} \mathbf{A}_{c,P} & \begin{pmatrix} -\frac{K_{1,0}}{C_0} & 0 & \dots & 0 \\ 0 & -\frac{K_{1,1}}{C_1} & \dots & 0 \\ \vdots & \vdots & \ddots & \vdots \\ 0 & 0 & \dots & -\frac{K_{1,n-1}}{C_{n-1}} \end{pmatrix} \\ -\mathbf{I}_n & \mathbf{0}_{n \times n} \end{pmatrix}, \quad (51)$$

$$\tilde{\mathbf{x}}(t) = (\mathbf{x}(t)^\top, \zeta_0(t), \zeta_1(t), \dots, \zeta_{n-1}(t))^\top, \quad (52)$$

where  $K_{P,j}$  is as in (45) and

$$K_{I,j} := \sum_{k=0}^{o_j-1} K_{I,j,k} \quad (53)$$

was summarized (without loss of generality). Again, the system is stable, if the real parts of all eigenvalues of  $\mathbf{A}_{c,PI}$  are negative, and if the disturbance  $\mathbf{d}(\mathbf{x}(t), \mathbf{u}_1(t), t)$  is bounded (which could be guaranteed by bounding  $\mathbf{u}_1(t)$  with dependency on  $\mathbf{x}(t)$ , see Remark 2). A simple analytical solution of the eigenvalues was found using Matlab's Symbolic Toolbox for the special (but meaningful) case  $\forall j: C_j = C, K_{P,j} = K_P, K_{I,j} = K_I$  for which the  $2n$  eigenvalues of  $\mathbf{A}_{c,PI}$  are given by

$$\left. \begin{aligned} \lambda_0 &= \frac{R_{te}K_P \mp n \pm \sqrt{(R_{te}K_P - n)^2 + 4K_I C R_{te}^2}}{2R_{te}C} \\ \text{for } n > 1, \forall j < n: \lambda_j &= \frac{K_P \pm \sqrt{K_P^2 + 4K_I C}}{2C} \end{aligned} \right\} \quad (54)$$

After some manipulations, the conditions (35)–(36) can be found analytically for stability  $\forall j: \Re\{\lambda_j\} < 0$ . ■

Further, it can be shown that a steady-state disturbance does not lead to a steady-state voltage error in case of PI-controllers.

ACKNOWLEDGMENTS

This study received funding from “Bund der Freunde der TU München e.V.” and from the European Union's Horizon 2020 research and innovation programme under the Marie Skłodowska-Curie grant agreement No 642682. The authors also want to thank the master student Zhenhan Xu for his work on the ESCs, superimposed flight controllers and assistance during experiments. The authors also want to thank Nadine Stappenbeck for her assistance during experiments.

REFERENCES

- [1] M. L. Loyd, “Crosswind kite power,” *Journal of Energy*, vol. 4, no. 3, pp. 106–111, 1980.
- [2] U. Ahrens, M. Diehl, and R. Schmehl, Eds., *Airborne Wind Energy*. Berlin Heidelberg: Springer, 2013.
- [3] J. W. Kolar, T. Friedli, F. Krismer, A. Looser, M. Schweizer, P. Steimer, and J. Bevirt, “Conceptualization and multi-objective optimization of the electric system of an airborne wind turbine,” in *Industrial Electronics (ISIE), 2011 IEEE International Symposium on*, June 2011, pp. 32–55.
- [4] Makani Power/Google. [Online]. Available: <https://www.google.com/makani/>
- [5] S. Nishikata and F. Tatsuta, “A new interconnecting method for wind turbine/generators in a wind farm and basic characteristics of the integrated system,” in *Power Electronics and Motion Control Conference, 2008. EPE-PEMC 2008. 13th*, Sept 2008, pp. 2343–2348.
- [6] D. Jovic, “Offshore wind farm with a series multiterminal CSI HVDC,” *Electric Power Systems Research*, vol. 78, no. 4, pp. 747 – 755, 2008. [Online]. Available: <http://www.sciencedirect.com/science/article/pii/S0378779607001332>
- [7] M. Popat, B. Wu, and N. R. Zargari, “Dc link current control of cascaded current source converter based offshore wind farms,” in *2011 IEEE International Electric Machines Drives Conference (IEMDC)*, May 2011, pp. 807–812.
- [8] S. Lundberg, “Wind farm configuration and energy efficiency studies - series DC versus AC layouts,” Ph.D. dissertation, Department of Energy and Environment, Chalmers University of Technology, 2006.
- [9] C. Meyer, “Key components for future offshore DC grids,” Ph.D. dissertation, Institute for Power Electronics and Electrical Drives, RWTH Aachen University, 2007.
- [10] G. Ortiz, J. Biela, D. Bortis, and J. W. Kolar, “1 Megawatt, 20 kHz, isolated, bidirectional 12kV to 1.2kV DC-DC converter for renewable energy applications,” in *Power Electronics Conference (IPEC), 2010 International*, June 2010, pp. 3212–3219.
- [11] R. Mahony, V. Kumar, and P. Corke, “Multirotor aerial vehicles: Modeling, estimation, and control of quadrotor,” *IEEE Robotics Automation Magazine*, vol. 19, no. 3, pp. 20–32, Sept 2012.
- [12] G. Ducard and M.-D. Hua, “Discussion and practical aspects on control allocation for a multi-rotor helicopter,” in *Proceedings of the 1st International Conference on UAVs in Geomatics, UAV-g 2011, Zurich, Switzerland*, 2011.
- [13] M. W. Achtelik, S. Lynen, M. Chli, and R. Siegwart, “Inversion based direct position control and trajectory following for micro aerial vehicles,” in *2013 IEEE/RSJ International Conference on Intelligent Robots and Systems*, Nov 2013, pp. 2933–2939.
- [14] T. Schneider, “Fault-tolerant multirotor systems,” Master Thesis, ETH Zürich, Department of Mechanical and Process Engineering, Institute of Robotics and Intelligent Systems, Autonomous Systems Lab, 2011. [Online]. Available: <https://pdfs.semanticscholar.org/7e1a/ecbf4acadc011be17b42242a430f16121191.pdf>
- [15] S. Jeon, J. J. Yun, and S. Bae, “Active cell balancing circuit for series-connected battery cells,” in *2015 9th International Conference on Power Electronics and ECCE Asia (ICPE-ECCE Asia)*, June 2015, pp. 1182–1187.
- [16] K. H. Nam, *AC Motor Control and Electrical Vehicle Applications*. CRC Press, 2010.
- [17] E. R. Magsino, C. M. Dollosa, S. Gavinio, G. Hermoso, N. Laco, and L. A. Roberto, “Stabilizing quadrotor altitude and attitude through speed and torque control of bldc motors,” in *2014 13th International Conference on Control Automation Robotics Vision (ICARCV)*, Dec 2014, pp. 438–443.
- [18] R. Martinez-Alvarado, F. J. Ruiz-Sanchez, A. Sanchez-Orta, and O. Garcia-Salazar, “Dynamic response of bldc-thruster for small scale quadrotors under aerodynamic load torque,” in *2014 IEEE International Autumn Meeting on Power, Electronics and Computing (ROPEC)*, Nov 2014, pp. 1–6.
- [19] C. Dirscherl, C. M. Hackl, and K. Schechner, “Modellierung und Regelung von modernen Windkraftanlagen: Eine Einführung,” in *Elektrische Antriebe – Regelung von Antriebssystemen*, 4th ed., D. Schröder, Ed. Springer, Berlin, 2015, pp. 1540–1614.
- [20] K. Schechner, F. Bauer, and C. M. Hackl, “Nonlinear DC-link PI control for airborne wind energy systems during pumping mode,” in *Airborne Wind Energy*, R. Schmehl, Ed. Springer, Singapore, 2017, accepted for publication.
- [21] L. Fagiano, K. Huynh, B. Bamieh, and M. Khammash, “On sensor fusion for airborne wind energy systems,” *IEEE Transactions on Control Systems Technology*, vol. 22, no. 3, pp. 930–943, May 2014.



**Florian Bauer** (M'16-S'17) was born in Germany in 1988. He received the B.Eng. degree in renewable energies from Fachhochschule Bielefeld, University of Applied Sciences, Bielefeld, Germany, in 2012, and the M.Sc. degree in electrical engineering and information technology from the Technical University of Munich (TUM), Munich, Germany, in 2013, where he is currently pursuing the Ph.D. degree with the Institute for Electrical Drive Systems and Power Electronics.

From 2014 to 2016, he was a Visiting Scholar with the Power Electronics Laboratory, University of California, Irvine, Irvine, CA, USA. Since 2014, he has been a Researcher with the Institute for Electrical Drive Systems and Power Electronics, TUM. His current research interests include kite power concepts, interconnection of electrical drives of airborne wind turbines, aerodynamics, flight system dynamics, and flight control. He has co-authored several publications for international conferences, journals, and book chapters about these topics.



**Christoph M. Hackl** (M'12-SM'16) was born in Mannheim, Germany, in 1977. After studying electrical engineering (controls and mechatronics) at Technical University of Munich (TUM, Germany) and University of Wisconsin-Madison (USA), he received the B.Sc., Dipl.-Ing., and Dr.-Ing. (Ph.D.) degree in 2003, 2004 and 2012, respectively.

Since 2004, he is teaching modeling and control of electrical drive, mechatronic and renewable energy systems at TUM. After a post-doc phase at the Institute of Electrical Drive Systems and Power

Electronics (EAL, TUM), he was appointed junior research fellow of the Munich School of Engineering (MSE, TUM) in 2014. He is heading the research group "Control of Renewable Energy Systems (CRES)" and is team leader of the "Renewable Energy Systems" group at EAL. His main research interests are nonlinear, adaptive and optimal control of electrical drive, mechatronic and renewable energy systems.



**Keyue Ma Smedley** (S'87-M'90-SM'97-F'08) received the B.S. and M.S. degrees in electrical engineering from Zhejiang University, Hangzhou, China, in 1982 and 1985, respectively, and the M.S. and Ph.D. degrees in electrical engineering from the California Institute of Technology, Pasadena, CA, USA, in 1987 and 1991, respectively.

She is currently a Professor at the Department of Electrical Engineering and Computer Science, University of California, Irvine (UCI), CA, USA, the Director of the UCI Power Electronics Laboratory, and cofounder of One-Cycle Control, Inc. Her research interests include high-efficiency DC-DC converters, high-fidelity class-D power amplifiers, PFC rectifiers, active power filters, inverters, V/VAR control, energy storage systems, and utility-scale fault current limiters. She is an inventor of one-cycle control and the hexagram power converter. Her work has resulted in more than 160 technical publications, more than 10 U.S./international patents, two start-up companies, and numerous commercial applications.



**Ralph M. Kennel** (M'90-SM'96) received the diploma degree in 1979 and the Dr.-Ing. degree in 1984 from the University of Kaiserslautern, Germany.

From 1983 to 1999, he worked on several positions with Robert BOSCH GmbH, Stuttgart, Germany. Until 1997, he was responsible for the development of servo drives. From 1994 to 1999, he was a Visiting Professor at the University of Newcastle-upon-Tyne, England, U.K. From 1999 to 2008, he was a Professor for electrical drives at Wuppertal University, Germany.

Since 2008, he has been a Professor for electrical drive systems and power electronics at Technical University of Munich, Germany. His main interests are sensorless control of AC drives, predictive control of power electronics, and hardware-in-the-loop systems.

Dr. Kennel is a Fellow of the IET, a Chartered Engineer in the U.K and IEEE Treasurer of Region 8. Dr. Kennel received the Harry Owen Distinguished Service Award from IEEE-PELS in 2013 and the EPE Association Distinguished Service Award in 2015.